Cluster State Generation with Spin-Orbit Coupled Fermionic Atoms in Optical Lattices

M. Mamaev,[1,2] R. Blatt,[3,4] J. Ye,[1] and A. M. Rey[1,2]
[1]JILA, NIST and Department of Physics, University of Colorado, Boulder, Colorado 80309, USA
[2]Center for Theory of Quantum Matter, University of Colorado, Boulder, Colorado 80309, USA
[3]Institute for Quantum Optics and Quantum Information, Austrian Academy of Sciences, Technikerstraße 21a, 6020 Innsbruck, Austria
[4]Institut für Experimentalphysik, Universität Innsbruck, Technikerstraße 25, 6020 Innsbruck, Austria

(Received 21 December 2018; published 24 April 2019)

Measurement-based quantum computation, an alternative paradigm for quantum information processing, uses simple measurements on qubits prepared in cluster states, a class of multiparty entangled states with useful properties. Here we propose and analyze a scheme that takes advantage of the interplay between spin-orbit coupling and superexchange interactions, in the presence of a coherent drive, to deterministically generate macroscopic arrays of cluster states in fermionic alkaline earth atoms trapped in three dimensional (3D) optical lattices. The scheme dynamically generates cluster states without the need of engineered transport, and is robust in the presence of holes, a typical imperfection in cold atom Mott insulators. The protocol is of particular relevance for the new generation of 3D optical lattice clocks with coherence times >10 s, 2 orders of magnitude larger than the cluster state generation time. We propose the use of collective measurements and time reversal of the Hamiltonian to benchmark the underlying Ising model dynamics and the generated many-body correlations.

DOI: 10.1103/PhysRevLett.122.160402

Entanglement, the characteristic trait of quantum mechanics, is a vital resource for quantum information processing [1], quantum communications [2], and enhanced metrology [3]. These applications often require multipartite entangled states, which can be difficult to create and intrinsically fragile to noise and decoherence. Nevertheless, there exists a special class of multipartite entangled states called cluster states, which can be robust to adverse effects on a subset of their logical qubits [4–6]. This intrinsic robustness, and the state entanglement properties, make cluster states in two (or three) dimensions a resource for one-way quantum computing, where a computation is realized by a sequence of single-qubit measurements on the initial cluster state. Besides their appeal in quantum computation, cluster states have been a playground for the study of many-body and statistical physics [6], graph theory [7], topological codes [8], and mathematical logic [9].

Cluster state generation has been reported in proof-of-principle experiments using frequency down-conversion techniques [10–12], photonic qubits [13,14], continuous-variable modes of squeezed light [15,16], semiconductor quantum dots [17], and trapped ions [18]. In addition, coherent entangling-disentangling evolution via controlled collisions was reported in cold atom Mott insulators [19], an experiment that stimulated theoretical work toward cluster state generation [20–24]. However, a scalable, deterministic source of cluster states needs yet to be realized.

Here we propose a scheme for preparing macroscopic cluster state arrays ($\sim 10^3$ qubits) in one, two, and three dimensions. Our protocol uses a combination of superexchange and spin-orbit coupling to engineer nearest-neighbor Ising interactions. In this implementation, cluster states naturally emerge during time evolution without the need of controlled collisions in spin dependent lattices [20], while maintaining robustness to imperfect filling. Although full tomography is not yet feasible in macroscopic systems, we propose the use of many-body echoes to probe the cluster state quality. Although our protocol is general and applicable to ultracold atomic systems interacting via contact [25] or engineered interactions (e.g., via an optical cavity) [26,27], it is particularly relevant for current 3D atomic lattice clocks [28–30] operated with fermionic alkaline earth atoms (AEs). These atoms offer untapped opportunities for precision metrology [31] and quantum information [30,32,33], because they possess a unique atomic structure featuring an ultranarrow clock transition with >100 s lifetimes, and a fully controllable, magnetic field insensitive hyperfine manifold. The demonstrated capability to generate spin-orbit coupling (SOC) in AEs [34–38], together with near-term experimentally accessible single-site addressability and control of SOC via accordion lattices [39–41], may enable the first realization of a large-scale one-way quantum computer in ultracold atoms using our protocol.

Model.—Consider N neutral fermionic atoms prepared in two long-lived internal states, denoted by g, e (e.g., optical

clock states or hyperfine nuclear spin states), trapped in a deep cubic optical lattice of L sites. We operate in the ultracold regime where only the lowest Bloch band is populated. The internal levels are continuously driven by a resonant laser (via optical or Raman transitions) with wave vector $\vec{k}_C$ and Rabi frequency $\Omega e^{i\vec{k}_C\cdot\vec{r}}$ at lattice position $\vec{r}$. The drive imprints a site-dependent phase $\phi_j = \vec{k}_C \cdot \vec{r}_j$, which transfers momentum to the atoms and generates spin-orbit coupling [34]. Here, $\vec{r}_j = (m, n, l)a$, with a the lattice spacing and m, n, l integers. By going to a dressed basis $\sigma \in \{\uparrow, \downarrow\}$ defined by the rotated states $|\uparrow\rangle = (|e\rangle - i|g\rangle)/\sqrt{2}$ and $|\downarrow\rangle = (|e\rangle + i|g\rangle)/\sqrt{2}$, (see the Supplemental Material, Sec. A [42]), the Hamiltonian is described by the following Fermi-Hubbard model ($\hbar = 1$)

$$\hat{H} = -J\sum_{\langle j,k\rangle,\sigma}(\hat{c}^\dagger_{j\sigma}\hat{c}_{k\sigma} + \text{H.c.}) + U\sum_j \hat{n}_{j\uparrow}\hat{n}_{j\downarrow} + \frac{\Omega}{2}\sum_j e^{i\pi j}(\hat{n}_{j\uparrow} - \hat{n}_{j\downarrow}). \quad (1)$$

Here, $\hat{c}_{j\sigma}$ annihilates an atom of spin σ on site j, $\hat{n}_{j\sigma} = \hat{c}^\dagger_{j\sigma}\hat{c}_{j\sigma}$, and $\langle j, k\rangle$ indices nearest-neighbors (no double counting). J is the hopping amplitude between sites, and $U > 0$ is the Hubbard repulsion [see Fig. 1(a)]. While the lattice is 3D, we can restrict this system to 1D or 2D by raising the confinement along the transverse direction(s). We have assumed that the phase between neighboring sites is $\phi_j - \phi_k = \pi$, corresponding to $a\vec{k}_C \cdot \hat{\alpha} = \pi$ for every unit vector $\hat{\alpha} \in \{\hat{x}, \hat{y}, \hat{z}\}$ along which tunneling is permitted, so that the sign of the Rabi drive alternates between neighbouring sites. This corresponds to inducing an effective gauge field with relative flux π, if one visualizes the spin as an additional synthetic dimension [43].

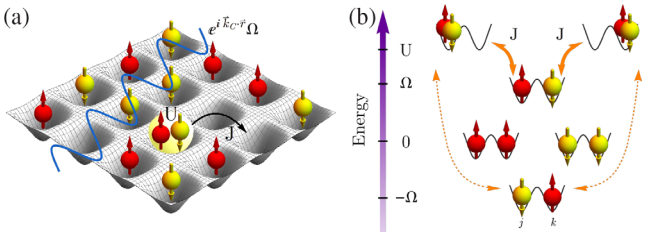

FIG. 1. (a) Schematic of the Fermi-Hubbard dynamics in an optical lattice, characterized by a nearest-neighbor tunneling energy J, and an onsite repulsion U. A resonant laser with Rabi frequency $\Omega e^{i\vec{k}_C\cdot\vec{r}}$ interrogates the internal levels while transferring momentum to the atoms (SOC). (b) Superexchange mechanism. The lowest(highest)-energy single-particle levels are in a staggered spin configuration due to the SOC. One type of virtual tunneling is suppressed by an energy cost $U + \Omega$, while another is near resonant with cost $U - \Omega$ (for $U \simeq \Omega$). Zero-energy states play no role due to Pauli exclusion prohibiting tunneling.

At half filling $N = L$, $\Omega/J \gg 1$ and $U/J \gg 1$, a Mott insulator is formed with suppression of doubly occupied sites. The strong drive favors staggered spin order and competes or cooperates with virtual second-order tunneling processes (superexchange). Instead of typical antiferromagnetic interactions [44,45], SOC transforms the Hamiltonian into a dominant nearest-neighbor Ising interaction. The underlying mechanism is depicted in Fig. 1(b). If two neighboring sites are in the single-particle ground state $|\downarrow\uparrow\rangle$, double occupancy after a tunneling event will cost an energy penalty $+\Omega$ due to the alternating Rabi drive, and an additional penalty $+U$ due to Hubbard repulsion, creating a large energy gap $\Omega + U$. If the particles are instead in the excited state $|\uparrow\downarrow\rangle$, virtual tunneling costs $-\Omega + U$ which can be made near resonant for $\Omega \simeq U$. The states $|\uparrow\uparrow\rangle$ and $|\downarrow\downarrow\rangle$ cannot tunnel due to Pauli exclusion. The effective superexchange Hamiltonian for our system (see the Supplemental Material, Sec. B [42]) becomes $\hat{H}_{\text{se}} = \hat{H}^{(1)}_{\text{se}} + \hat{H}^{(2)}_{\text{se}}$ with

$$\hat{H}^{(1)}_{\text{se}} \equiv \frac{4J^2U}{\Omega^2 - U^2}\sum_{\langle j,k\rangle}\hat{S}^z_j\hat{S}^z_k + \left(\Omega + \mathcal{D}\frac{4J^2\Omega}{\Omega^2 - U^2}\right)\sum_j \hat{S}^z_j, \quad (2)$$

where $\hat{S}^\alpha_j$ are spin-1/2 operators, and $\mathcal{D}$ is the dimensionality (i.e., $\mathcal{D} = 2$ for 2D tunneling). There is an additional interaction $\hat{H}^{(2)}_{\text{se}} \equiv (2J^2/U)\sum_{\langle j,k\rangle}(\hat{S}^+_j\hat{S}^+_k + \text{H.c.})$, but its contribution to unitary evolution is rendered negligible in our parameter regime by the SOC, which forces the states affected by $\hat{H}^{(2)}_{\text{se}}$ to pick up a high-frequency phase $\sim e^{-2i\Omega t}$ from the drive, making their off-diagonal terms in the unitary proportional to $\sim J^2/(\Omega U)$ and thus negligible (see the Supplemental Material, Sec. C [42]). The superexchange mapping is exact in the limit of $U/J \to \infty$, and $|\Omega - U|/J \to \infty$ to avoid higher-order processes (see the Supplemental Material, Sec. D [42] for benchmarking).

Cluster states.— A cluster state $|\psi_c\rangle$ is a many-body quantum resource state, characterized by localizable entanglement. It can be generated by applying a controlled phase gate on every pair of neighboring sites $\langle j, k\rangle$: $\exp[-i(\hat{S}^z_j\hat{S}^z_k + \frac{1}{2}\hat{S}^z_j + \frac{1}{2}\hat{S}^z_k)\pi]|\leftarrow\rangle_j|\leftarrow\rangle_k$ where $|\leftarrow\rangle_j = (|\uparrow\rangle_j - |\downarrow\rangle_j)/\sqrt{2}$ [see Fig. 2(a)]. Logic gates can be implemented by consecutive measurements on the cluster state, permitting a platform for quantum computation that needs no entanglement generation besides the initial state. A 2D cluster state is sufficient for universal computation [6], whereas a 3D state also has significant fault tolerance on the order of 25% error [46]. We propose to use the Ising interaction in Eq. (2) applied to an initial state $|\psi(0)\rangle = |\leftarrow, \leftarrow, \cdots \leftarrow\rangle$ to realize a cluster state. We bring the drive close to resonance, $\Omega \simeq U$, making the $\hat{S}^z_j\hat{S}^z_{j+1}$ term large enough to access cluster states on experimentally viable

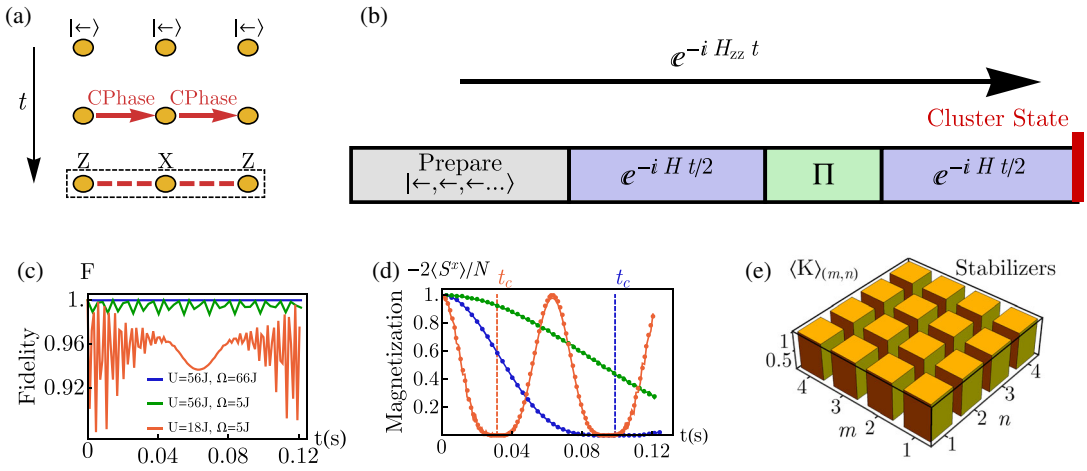

FIG. 2. (a) Cluster state schematic. Controlled phase gates are applied to nearest-neighbor pairs. The resulting correlations are local stabilizer operators (here in 1D). (b) Protocol for generating cluster states. The system is evolved with a spin echo to simulate an Ising interaction. (c) Fidelity $F = |\langle\psi(t)|\psi(t)\rangle_{zz}|^2$ between an Ising Hamiltonian evolution and our protocol from Eq. (3), using the superexchange model. Parameters are $J/(2\pi) = 28$ Hz for $U/J = 56$, and $J/(2\pi) = 66$ Hz for $U/J = 18$. System size is $L = 4 \times 4$ with 2D tunneling. (d) Time evolution of $\langle\hat{S}^x\rangle$ for our protocol (lines) and ideal Ising model (dots). Cluster times $t_c = \pi/J_{zz}$ are indicated in matching color. Note that t_c is shorter for the red line because it has a higher J, and thus higher $J_{zz} \sim J^2$. (e) 2D cluster correlations at half filling with $L = 4 \times 4$, $U/J = 56$, $\Omega/J = 66$.

timescales, as discussed in the last part of this Letter. The single-particle terms in the Hamiltonian can be removed with a spin echo: we evolve to a halfway time, make a π-pulse $\hat{\Pi} = e^{-i\pi\hat{S}^x}$ and evolve for the second half, undoing any on site rotations [see Fig. 2(b)]:

$$|\psi(t)\rangle_{zz} = e^{-i\hat{H}_{se}t/2}\hat{\Pi}e^{-i\hat{H}_{se}t/2}|\psi(0)\rangle \approx e^{-i\hat{H}_{zz}t}|\psi(0)\rangle,$$
$$\hat{H}_{zz} = J_{zz}\sum_{\langle j,k\rangle}\hat{S}^z_j\hat{S}^z_k, \qquad J_{zz} = \frac{4J^2U}{\Omega^2 - U^2}. \tag{3}$$

Evolving under the Ising interaction to the cluster time, $t_c = \pi/J_{zz}$ implements the controlled phase gates needed.

At half filling, the protocol prepares an almost perfect cluster state (up to single-particle rotations) for appropriate parameters. Figures 2(c) and 2(d) compare the protocol to the ideal Ising model with fidelity and collective $\hat{S}^x = \sum_j \hat{S}^x_j$ observables.

A cluster state $|\psi_c\rangle$ can be equivalently defined as an eigenstate of stabilizer operators [5]. These are local multibody operators that quantify the localizable entanglement in the state

$$\langle \mathrm{K}\rangle_j \equiv 2^{2\mathcal{D}+1}\langle\psi|\hat{S}^x_j\prod_{\langle j,k\rangle}\hat{S}^z_k|\psi\rangle = 1 \quad \text{for } |\psi\rangle = |\psi_c\rangle. \tag{4}$$

The closeness of these stabilizer expectation values, which we call cluster correlations hereafter, to $|\langle K\rangle_j| = 1$ in a given region of the lattice is a metric of the cluster state quality there [5]. There is no significant distinction between $\langle K\rangle_j = \pm 1$, because the two can be interchanged with an $\hat{S}^z$ rotation, and we take absolute values when all stabilizers are negative. In Fig. 2(e), we show stabilizers for the superexchange model in 2D at half filling. This acts as a better metric than global state fidelity, because the localized nature of cluster state entanglement still permits computation using a region of the lattice if some other, unconnected region is corrupted.

Imperfect Mott insulator.— A major source of error in experiments is the presence of vacancies in the initial state, which can move and disrupt the correlations. In our implementation they are kept localized by the staggered energy structure imposed by the drive [cf. Fig. 1(b)]. Tunneling into an adjacent empty site costs $\pm\Omega$ and is thus inhibited. Although an empty site still destroys the entanglement with its neighbors, other nonadjacent sites can maintain cluster correlations.

Figure 3(a) compares cluster correlations for a half-filling sample and a doped array for a 1D system (tunneling allowed along one direction). Sites away from the hole maintain high stabilizer values. A similar result is seen in Fig. 3(b) for 2D. Given the complexity of solving full Fermi-Hubbard dynamics in this case, we instead use an effective spin-1 model to account for holes (see the Supplemental Material, Sec. E [42]). Although that model overestimates the correlations at sites affected by the vacancies [see green plot in Fig. 3(a)], overall it shows that away from them the correlations persist.

In addition to the above benchmarks, we also compute robustness of stabilizers to increasing system size and external confinement (see the Supplemental Material, Sec. F [42]).

Collective cluster measurements and OTOCs.—Probing stabilizers directly requires measurements of multibody

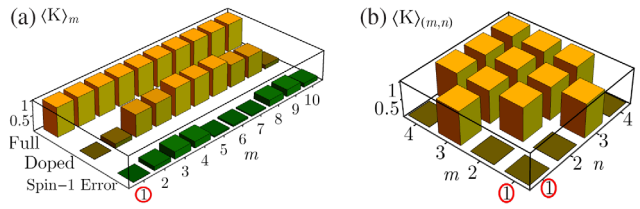

FIG. 3. (a) Cluster correlations for an $L = 10$ system with 1D tunneling at half filling (full), and with one vacancy initially on site $m = 1$ (doped). Orange plots are computed with Fermi-Hubbard. The green plots quantify how we would have overestimated the correlations if we had instead used an approximate spin-1 model (see the Supplemental Material, Sec. E [42]). Parameters are $J/(2\pi) = 22$ Hz, $U/J = 115$, $\Omega/J = 140$. (b) Cluster correlations for a 2D system $L = 4 \times 4$ with one vacancy at $(m, n) = (1, 1)$. The spin-1 is used due to the numerical complexity of the Fermi-Hubbard. Although it overestimates the correlations, qualitatively the hole remains localized. Parameters are $J/(2\pi) = 28$ Hz, $U/J = 56$, $\Omega/J = 66$.

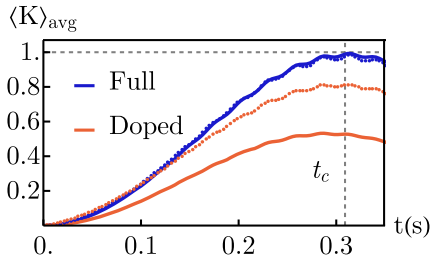

FIG. 4. Dynamics of average cluster correlations for a 1D tunneling lattice of $L = 8$, at half filling (blue) and one vacancy on site $j = 1$ (red), using Fermi-Hubbard. Solid lines generate the cluster state directly and measure the local correlators. We then average across all sites. Dotted lines use the time-reversal protocol of Eq. (5), relying upon only collective measurements of $\langle \hat{S}^x \rangle$. Parameters are $J/(2\pi) = 22$ Hz, $U/J = 115$, $\Omega/J = 140$.

correlations with single-site resolution. Although the resolution is required for one-way quantum information processing, at least for initial test-bed experiments, it is possible to partially bypass this requirement by using inherent properties in the Ising model combined with global probes. Notice that

$$\begin{aligned}\langle \mathrm{K} \rangle_j(t) &= 2^{2\mathcal{D}+1} \langle \psi(0)| e^{i\hat{H}_{zz}t} \left(\hat{S}_j^x \prod_{\langle j,k \rangle} \hat{S}_k^z \right) e^{-i\hat{H}_{zz}t} |\psi(0)\rangle, \\ &= 2(-1)^{\mathcal{D}} \langle \psi(0)| e^{i\hat{H}_{zz}t} (e^{-i\hat{H}_{zz}t_c} \hat{S}_j^x e^{i\hat{H}_{zz}t_c}) e^{-i\hat{H}_{zz}t} |\psi(0)\rangle, \end{aligned} \tag{5}$$

implying that the many-body measurement can be replaced with a local one by evolving to twice the cluster time instead (see the Supplemental Material, Sec. G [42]). Measuring over a region $\hat{S}_R^x = \sum_{j \in R} \hat{S}_j^x$ yields mean values of cluster correlations in R, which offers a metric for cluster state quality there. This does not contain information about the entire state, but is sufficient to gauge fidelity of computation using the region R. Although the sign of the Ising interaction inside the brackets of Eq. (5) does not matter, the time reversal of the Hamiltonian can be implemented, thanks to the tunability of the interaction, providing additional benchmarking capability and a more objective comparison.

After evolving to the cluster time, we quench the drive, $\Omega \to \sqrt{2U^2 - \Omega^2}$, causing the interaction to flip its sign, $\hat{H}_{zz} \to -\hat{H}_{zz}$ [the Ising model is realized with the spin echo of Eq. (3)]. If the mapping between the Fermi-Hubbard and superexchange were exact, then at $t = t_c$ we implement a unitary reversal and measure ideal cluster correlations. Doping or nonideal implementation of the Ising would yield lower values. Figure 4 compares the dynamics of cluster correlations with exact many-body measurements and the collective measurement $\langle \hat{S}^x \rangle(t)$ ($R = N$). With half filling, we see near-perfect agreement. For a doped array, the collective measurements overestimate the correlations, but still maintain the overall trend.

The goal of the above protocol is to gauge the cluster state quality. To actually implement quantum computation after cluster states are generated requires a nontrivial measurement sequence [47,48]. Because the focus of this work is cluster state generation instead of one-way quantum computation, we leave the details of the latter to future work.

As a side remark, the ability to generate time-reversed evolution allows us to measure out-of-time-ordered correlations (OTOCs) [49–51]. An OTOC is defined as $C_{WV}(t) = \langle \hat{W}(t)^\dagger \hat{V}^\dagger \hat{W}(t) \hat{V} \rangle$, where $\hat{W}, \hat{V}$ are commuting operators and $\hat{W}(t) = e^{i\hat{H}t} \hat{W} e^{-i\hat{H}t}$. OTOCs quantify how quantum information is scrambled over many-body degrees of freedom after a quench [49]. OTOCs have also been considered a proxy of quantum chaos [52]. In our system, OTOCs can be measured if we choose $\hat{V} = \hat{S}^x$, because $\langle \hat{W}(t)^\dagger \hat{V}^\dagger \hat{W}(t) \hat{V} \rangle = -L \langle \hat{W}(t)^\dagger \hat{V}^\dagger \hat{W}(t) \rangle / 2$, and $\hat{W} = e^{-i\theta \hat{S}^x}$ is a collective rotation for some angle θ, which is straightforward to realize experimentally. Different OTOCs can be measured by using different rotation axes or angles.

Experimental parameters and implementations.— One of the most promising systems to implement our proposal is the 3D optical lattice clock, operated with fermionic Strontium-87 atoms in a cubic lattice at the "magic-wavelength" $a \approx 406$ nm [53]. Along the directions where we want tunneling, we assume lattice confinement of $V_0/E_r \approx 15$–20 (E_r the recoil energy), to obtain $J \sim 10 \times 2\pi$Hz, and much deeper confinement $V_0/E_r \gtrsim 100$ along other directions. For a scattering length $a_{\mathrm{eg}}^- \approx 69 a_0$ [30] (a_0 the Bohr radius), the onsite interaction strength is $U/J \sim 100$. The Rabi frequency needs to satisfy both $\Omega \simeq U$ and $|U - \Omega|/J \gg 1$ to allow fast cluster state generation $t_c \sim 0.1$ s compared to the current experimental coherence

time of ~10 s [30] (limited by light scattering), and to guarantee the validity of the superexchange model.

The spin degree of freedom can be encoded in the two long-lived $^1S_0(g) - {}^3P_0(e)$ clock states in a nuclear-spin polarized gas. Pauli exclusion prevents undesirable *e-e* inelastic collisions in the lowest band.

The achievable SOC phase depends on $|\vec{k}_C| = 2\pi/\lambda_C$, with λ_C the transition wavelength. For the $^1S_0 - {}^3P_0$ states in the magic-wavelength lattice, the $\lambda_C \approx 698$ nm clock laser naturally imparts the required SOC. To achieve the necessary π phase in 1D, one needs to suppress tunneling along the $\hat{y}$, $\hat{z}$ lattice directions, enable tunneling along $\hat{x}$ and incline the laser so that $a\vec{k}_C \cdot \hat{x} = \pi$. For 2D, one enables tunneling along $\hat{x}$, $\hat{y}$, points the laser in that plane at 45°, and likewise inclines until the projection along both equals π. Although the current magic wavelength lattice requires a slightly larger $|\vec{k}_C|$ for 2D, it can be adjusted through the use of accordion lattices to increase a [41], or by using a separate laser for each axis.

Alternatively, one can use two nuclear-spin states in the $^1S_0$ ground state manifold and Raman transitions to generate the desired SOC, with the one-photon detuning of the Raman lasers set sufficiently large to enable a long coherence time [54]. In particular, the $^1S_0 - {}^1P_1$ at $\lambda_C \approx 461$ nm is appealing because it naturally realizes a SOC phase difference of $\approx\pi$ in each direction when the laser is oriented along the (1,1,1) spatial axis, providing the framework for a 3D cluster state.

Conclusions and outlook.— We proposed a protocol to generate macroscopic cluster states in 3D lattice arrays of ultracold atoms via dynamical evolution. The progress of individual atom control and manipulation offered by quantum gas microscopes [55,56], optical tweezers [57], as well as the recent capability of micron-resolution spatial imaging with submillihertz frequency resolution in optical lattice clocks [28] are already allowing experiments to prepare the high-fidelity Mott insulators needed for high quality cluster states. Combined with long-coherent times offered by AEs, our protocol can open a path for first proof-of-principle demonstrations of one-way computing schemes in the near future.

M. M. and A. M. R. acknowledge helpful discussions from M. A. Perlin, S. R. Muleady, and P. He. M. M. acknowledges funding from the Center for Theory of Quantum Matter graduate fellowship. R. B. acknowledges a visiting fellowship at JILA. This work is supported by the Air Force Office of Scientific Research Grant No. FA9550-18-1-0319 and its Multidisciplinary University Research Initiative grant, by the Defense Advanced Research Projects Agency and Army Research Office Grant No. W911NF-16-1-0576, the National Science Foundation Grant No. PHY-1820885, JILA-NSF Grant No. PFC-173400, and the National Institute of Standards and Technology.

[1] M. A. Nielsen and I. Chuang, Quantum computation and quantum information (Cambridge University Press, New York, 2000).
[2] N. Gisin, G. Ribordy, W. Tittel, and H. Zbinden, Quantum cryptography, Rev. Mod. Phys. **74**, 145 (2002).
[3] C. F. Roos, M. Chwalla, K. Kim, M. Riebe, and R. Blatt, 'Designer atoms' for quantum metrology, Nature (London) **443**, 316 (2006).
[4] R. Raussendorf and H. J. Briegel, A One-Way Quantum Computer, Phys. Rev. Lett. **86**, 5188 (2001).
[5] R. Raussendorf, D. E Browne, and H. J Briegel, Measurement-based quantum computation on cluster states, Phys. Rev. A **68**, 022312 (2003).
[6] H. J. Briegel, D. E. Browne, W. Dür, R. Raussendorf, and M. Van den Nest, Measurement-based quantum computation, Nat. Phys. **5**, 19 (2009).
[7] M. Hein, J. Eisert, and H. J Briegel, Multiparty entanglement in graph states, Phys. Rev. A **69**, 062311 (2004).
[8] R. Raussendorf, J. Harrington, and K. Goyal, Topological fault-tolerance in cluster state quantum computation, New J. Phys. **9**, 199 (2007).
[9] M. Van den Nest and H. J. Briegel, Measurement-based quantum computation and undecidable logic, Found. Phys. **38**, 448 (2008).
[10] M. Chen, N. C. Menicucci, and O. Pfister, Experimental Realization of Multipartite Entanglement of 60 Modes of a Quantum Optical Frequency Comb, Phys. Rev. Lett. **112**, 120505 (2014).
[11] C.-Y. Lu, X.-Q. Zhou, O. Gühne, W.-B. Gao, J. Zhang, Z.-S. Yuan, A. Goebel, T. Yang, and J.-W. Pan, Experimental entanglement of six photons in graph states, Nat. Phys. **3**, 91 (2007).
[12] P. Walther, K. J. Resch, T. Rudolph, E. Schenck, H. Weinfurter, V. Vedral, M. Aspelmeyer, and A. Zeilinger, Experimental one-way quantum computing, Nature (London) **434**, 169 (2005).
[13] K. Chen, C.-M. Li, Q. Zhang, Y.-A. Chen, A. Goebel, S. Chen, A. Mair, and J.-W. Pan, Experimental Realization of One-Way Quantum Computing with Two-Photon Four-Qubit Cluster States, Phys. Rev. Lett. **99**, 120503 (2007).
[14] N. Kiesel, C. Schmid, U. Weber, G. Tóth, O. Gühne, R. Ursin, and H. Weinfurter, Experimental Analysis of a Four-Qubit Photon Cluster State, Phys. Rev. Lett. **95**, 210502 (2005).
[15] S. Yokoyama, R. Ukai, S. C. Armstrong, C. Sornphiphatphong, T. Kaji, S. Suzuki, J.-i. Yoshikawa, H. Yonezawa, N. C. Menicucci, and A. Furusawa, Ultra-large-scale continuous-variable cluster states multiplexed in the time domain, Nat. Photonics **7**, 982 (2013).
[16] M. Yukawa, R. Ukai, P. van Loock, and A. Furusawa, Experimental generation of four-mode continuous-variable cluster states, Phys. Rev. A **78**, 012301 (2008).
[17] I. Schwartz, D. Cogan, E. R. Schmidgall, Y. Don, L. Gantz, O. Kenneth, N. H. Lindner, and D. Gershoni, Deterministic generation of a cluster state of entangled photons, Science **354**, 434 (2016).
[18] B. P. Lanyon, P. Jurcevic, M. Zwerger, C. Hempel, E. A. Martinez, W. Dür, H. J. Briegel, R. Blatt, and C. F. Roos, Measurement-Based Quantum Computation with Trapped Ions, Phys. Rev. Lett. **111**, 210501 (2013).

[19] O. Mandel, M. Greiner, A. Widera, T. Rom, T. W. Hänsch, and I. Bloch, Controlled collisions for multi-particle entanglement of optically trapped atoms, Nature (London) **425**, 937 (2003).
[20] A. J. Daley, M. M. Boyd, J. Ye, and P. Zoller, Quantum Computing with Alkaline-Earth-Metal Atoms, Phys. Rev. Lett. **101**, 170504 (2008).
[21] B. Vaucher, A. Nunnenkamp, and D. Jaksch, Creation of resilient entangled states and a resource for measurement-based quantum computation with optical superlattices, New J. Phys. **10**, 023005 (2008).
[22] E. Kuznetsova, T. Bragdon, R. Côté, and S. F. Yelin, Cluster-state generation using van der waals and dipole-dipole interactions in optical lattices, Phys. Rev. A **85**, 012328 (2012).
[23] P. Treutlein, T. Steinmetz, Y. Colombe, B. Lev, P. Hommelhoff, J. Reichel, M. Greiner, O. Mandel, A. Widera, T. Rom *et al.*, Quantum information processing in optical lattices and magnetic microtraps, Fortschr. Phys. **54**, 702 (2006).
[24] M. Zwierz and P. Kok, High-efficiency cluster-state generation with atomic ensembles via the dipole-blockade mechanism, Phys. Rev. A **79**, 022304 (2009).
[25] C. Gross and I. Bloch, Quantum simulations with ultracold atoms in optical lattices, Science **357**, 995 (2017).
[26] R. Landig, L. Hruby, N. Dogra, M. Landini, R. Mottl, T. Donner, and T. Esslinger, Quantum phases from competing short-and long-range interactions in an optical lattice, Nature (London) **532**, 476 (2016).
[27] A. Camacho-Guardian, R. Paredes, and S. F. Caballero-Benítez, Quantum simulation of competing orders with fermions in quantum optical lattices, Phys. Rev. A **96**, 051602(R) (2017).
[28] S. L. Campbell, R. B. Hutson, G. E. Marti, A. Goban, N. Darkwah Oppong, R. L. McNally, L. Sonderhouse, J. M. Robinson, W. Zhang, B. J. Bloom *et al.*, A fermi-degenerate three-dimensional optical lattice clock, Science **358**, 90 (2017).
[29] G. E. Marti, R. B. Hutson, A. Goban, S. L. Campbell, N. Poli, and J. Ye, Imaging Optical Frequencies with 100 μhz Precision and 1.1 μm Resolution, Phys. Rev. Lett. **120**, 103201 (2018).
[30] A. Goban, R. B. Hutson, G. E. Marti, S. L. Campbell, M. A. Perlin, P. S. Julienne, J. P. D'Incao, A. M. Rey, and J. Ye, Emergence of multi-body interactions in a fermionic lattice clock, Nature (London) **563**, 369 (2018).
[31] A. D. Ludlow, M. M. Boyd, J. Ye, E. Peik, and P. O. Schmidt, Optical atomic clocks, Rev. Mod. Phys. **87**, 637 (2015).
[32] A. J. Daley, Quantum computing and quantum simulation with group-II atoms, Quantum Inf. Process. **10**, 865 (2011).
[33] M. A. Cazalilla and A. M. Rey, Ultracold fermi gases with emergent SU(N) symmetry, Rep. Prog. Phys. **77**, 124401 (2014).
[34] M. L. Wall, A. P. Koller, S. Li, X. Zhang, N. R. Cooper, J. Ye, and A. M. Rey, Synthetic Spin-Orbit Coupling in an Optical Lattice Clock, Phys. Rev. Lett. **116**, 035301 (2016).
[35] S. Kolkowitz, S. L. Bromley, T. Bothwell, M. L. Wall, G. E. Marti, A. P. Koller, X. Zhang, A. M. Rey, and J. Ye, Spin–orbit-coupled fermions in an optical lattice clock, Nature (London) **542**, 66 (2017).
[36] S. L. Bromley, S. Kolkowitz, T. Bothwell, D. Kedar, A. Safavi-Naini, M. L. Wall, C. Salomon, A. M. Rey, and J. Ye, Dynamics of interacting fermions under spin–orbit coupling in an optical lattice clock, Nat. Phys. **14**, 399 (2018).
[37] L. F. Livi, G. Cappellini, M. Diem, L. Franchi, C. Clivati, M. Frittelli, F. Levi, D. Calonico, J. Catani, M. Inguscio *et al.*, Synthetic Dimensions and Spin-Orbit Coupling with an Optical Clock Transition, Phys. Rev. Lett. **117**, 220401 (2016).
[38] V. Galitski and I. B. Spielman, Spin–orbit coupling in quantum gases, Nature (London) **494**, 49 (2013).
[39] S. Al-Assam, R. A. Williams, and C. J. Foot, Ultracold atoms in an optical lattice with dynamically variable periodicity, Phys. Rev. A **82**, 021604(R) (2010).
[40] R. A. Williams, J. D. Pillet, S. Al-Assam, B. Fletcher, M. Shotter, and C. J. Foot, Dynamic optical lattices: Two-dimensional rotating and accordion lattices for ultracold atoms, Opt. Express **16**, 16977 (2008).
[41] Y. Hudson *et al.*, Engineering quantum states of matter for atomic clocks in shallow optical lattices, arXiv:1903.02498.
[42] See Supplemental Material at http://link.aps.org/supplemental/10.1103/PhysRevLett.122.160402 for derivations of the Hamiltonians and numerical techniques used, as well as additional benchmarking comparisons.
[43] A. Celi, P. Massignan, J. Ruseckas, N. Goldman, I. B. Spielman, G. Juzeliūnas, and M. Lewenstein, Synthetic Gauge Fields in Synthetic Dimensions, Phys. Rev. Lett. **112**, 043001 (2014).
[44] P. W. Anderson, Antiferromagnetism. Theory of superexchange interaction, Phys. Rev. **79**, 350 (1950).
[45] S. Trotzky, P. Cheinet, S. Fölling, M. Feld, U. Schnorrberger, A. M. Rey, A. Polkovnikov, E. A. Demler, M. D. Lukin, and I. Bloch, Time-resolved observation and control of superexchange interactions with ultracold atoms in optical lattices, Science **319**, 295 (2008).
[46] S. D. Barrett and T. M. Stace, Fault Tolerant Quantum Computation with Very High Threshold for Loss Errors, Phys. Rev. Lett. **105**, 200502 (2010).
[47] R. Raussendorf and H. Briegel, Computational model underlying the one-way quantum computer, Quantum Inf. Comput. **6**, 433 (2002).
[48] V. Danos, E. Kashefi, and P. Panangaden, The measurement calculus, J. ACM **54**, 8 (2007).
[49] S. H. Shenker and D. Stanford, Black holes and the butterfly effect, J. High Energy Phys. 03 (2014) 067.
[50] B. Swingle, G. Bentsen, M. Schleier-Smith, and P. Hayden, Measuring the scrambling of quantum information, Phys. Rev. A **94**, 040302(R) (2016).
[51] M. Gärttner, J. G. Bohnet, A. Safavi-Naini, M. L. Wall, J. J. Bollinger, and A. M. Rey, Measuring out-of-time-order correlations and multiple quantum spectra in a trapped-ion quantum magnet, Nat. Phys. **13**, 781 (2017).
[52] J. Maldacena, S. H. Shenker, and D. Stanford, A bound on chaos, J. High Energy Phys. 08 (2016) 106.
[53] J. Ye, H. J. Kimble, and H. Katori, Quantum state engineering and precision metrology using state-insensitive light traps, Science **320**, 1734 (2008).
[54] M. Mancini, G. Pagano, G. Cappellini, L. Livi, M. Rider, J. Catani, C. Sias, P. Zoller, M. Inguscio, M. Dalmonte *et al.*,

Observation of chiral edge states with neutral fermions in synthetic hall ribbons, Science **349**, 1510 (2015).

[55] W. S. Bakr, J. I. Gillen, A. Peng, S. Fölling, and M. Greiner, A quantum gas microscope for detecting single atoms in a hubbard-regime optical lattice, Nature (London) **462**, 74 (2009).

[56] M. F. Parsons, F. Huber, A. Mazurenko, C. S. Chiu, W. Setiawan, K. Wooley-Brown, S. Blatt, and M. Greiner, Site-Resolved Imaging of Fermionic ^{6}Li in an Optical Lattice, Phys. Rev. Lett. **114**, 213002 (2015).

[57] M. Endres, H. Bernien, A. Keesling, H. Levine, E. R. Anschuetz, A. Krajenbrink, C. Senko, V. Vuletic, M. Greiner, and M. D. Lukin, Atom-by-atom assembly of defect-free one-dimensional cold atom arrays, Science **354**, 1024 (2016).